Temperature shifts in the Sinai model: static and dynamical effects

2003 J. Phys. A: Math. Gen. 36 665

(http://iopscience.iop.org/0305-4470/36/3/306)

INSTITUTE OF PHYSICS PUBLISHING JOURNAL OF PHYSICS A: MATHEMATICAL AND GENERAL

J. Phys. A: Math. Gen. **36** (2003) 665–684 PII: S0305-4470(03)39536-8

Temperature shifts in the Sinai model: static and dynamical effects

Marta Sales[1], **Jean-Philippe Bouchaud**[2] **and Fèlix Ritort**[1]

[1] Departament de Física Fonamental, Facultat de Física, Universitat de Barcelona, Diagonal 647, 08028 Barcelona, Spain
[2] Service de Physique de l'État Condensé, Centre d'études de Saclay, Orme des Merisiers, 91191 Gif-sur-Yvette Cedex, France

Received 12 July 2002, in final form 8 October 2002
Published 7 January 2003
Online at stacks.iop.org/JPhysA/36/665

Abstract

We study analytically and numerically the role of temperature shifts in the simplest model where the energy landscape is explicitly hierarchical, namely the Sinai model. This model has both attractive features (there are valleys within valleys in a strict self-similar sense), but also one important drawback: there is no phase transition so that the model is, in the large-size limit, effectively at zero temperature. We compute various static chaos indicators, that are found to be trivial in the large-size limit, but exhibit interesting features for finite sizes. Correspondingly, for finite times, some interesting rejuvenation effects, related to the self-similar nature of the potential, are observed. Still, the separation of time scales/length scales with temperature in this model is much weaker than in experimental spin glasses.

PACS numbers: 75.10.Nr, 75.40.Gb, 75.40.Mg

1. Introduction

The phenomenology of very different glassy systems (spin glasses, structural glasses, pinned defects) exhibits striking similarities. This is often discussed in terms of a complex energy landscape, with some universal features in the organization of valleys, saddles and barriers [1–4]. Mean-field models suggest that the energy landscape of some systems is hierarchical, with a self-similar organization of valleys within valleys [5]. This picture has been advocated to interpret [6–8] the striking rejuvenation and memory effects during temperature cycling experiments, observed first in spin glasses, but also in disordered ferromagnets, dipolar glasses, polymer glasses (PMMA) or gelatin [10–13]. These experiments study the effects of temperature shifts, $T_1 \to T_2 < T_1 \to T_1$ on the aging part of the susceptibility. *Rejuvenation* describes the restart of the aging process observed upon changing the temperature to T_2 after having aged at temperature T_1: the relaxation curve at T_2 is indeed, to a good approximation, identical to that measured after a direct quench from high temperature to T_2. *Memory*, on the other hand, means that the aging process observed when the system is set back to T_1 resumes as if no shift had occurred.

Another general framework to understand disordered systems is the droplet picture, developed in the context of spin glasses and of pinned manifolds (domain walls, vortices, etc) [14, 15]. The approach aims at describing the physics in terms of localized excitations of different sizes (droplets), with an energy scale that grows with their size. As emphasized in [16, 17], these two approaches are in fact complementary, and the dynamics in the droplet model is naturally hierarchical, due to the strong separation of time scales with length scales and temperature. Temperature plays the role of a microscope since the active length scales that contribute to the dynamics are very different at different temperatures.

In both pictures, memory conservation is due to this separation of time scales with temperature [18, 19] (see also [20]). The origin of *rejuvenation*, however, is different. In the hierarchical landscape framework, a small temperature drop (from T_1 to $T_2 = T_1 - \Delta T$) reveals finer details of the random energy landscape, among which the system must reequilibrate. In other words, small length scales, that are 'unpinned' at temperature T_1, freeze at T_2, thereby producing a strong out of equilibrium signal (rejuvenation). This scenario can be given some precise meaning in the context of the random energy model (REM) close to its critical temperature [21], or in the generalized (multilevel) REM where rejuvenation and memory effects very similar to experiments can indeed be observed [22, 23]. On the other hand, rejuvenation effects in the droplet model have been attributed to 'temperature chaos': for any temperature difference ΔT, the equilibrium configurations at the two temperatures are completely different beyond a certain length scale $\ell_{\Delta T}$, called the overlap length, that diverges when $\Delta T \to 0$ as a power law. Correspondingly, the correlations of the free energies at the two temperatures are thought to decay with the size of the system L as $\exp(-L/\ell_{\Delta T})$. This scenario, postulated for spin glasses in [14, 15], has been given credit recently in the context of directed polymers [24–26]. In this case, both analytical arguments and numerical results point towards the existence of an overlap length, although the free-energy decorrelation appears to be much slower than exponential in the size of the system. For spin glasses, the status of temperature chaos is still controversial and unclear as compared to the influence of other, stronger perturbations such as magnetic field changes or coupling strength changes. Results in mean-field spin glasses [27–29] and numerical calculations for small systems [30] hint at extremely weak chaotic effects in temperature. This conclusion extends also to short-range systems where chaotic effects in the equilibrium properties seem to be extremely weak [31, 32]. Chaotic effects, if any, seem to appear only for quite large systems even when $\Delta T/T$ is of order one [33–35]. Nevertheless, some recent spin-glass experiments were interpreted in terms of an overlap length [36], whereas numerical simulations of the 4D Edwards–Anderson model have revealed rejuvenation due to small scale freezing without chaos [19]. (For a detailed study in the 3D Edwards–Anderson model and a discussion of possible scenarios about why rejuvenation effects are not observed in simulations, see [19, 37].)

In view of the controversy, we feel that more work on the subject is needed. The aim of the present paper is to study in detail the question of 'temperature chaos' on the Sinai model, which is the simplest model where the energy landscape is *explicitly hierarchical*, and for which many exact results are available [38–42]. The Sinai model was discussed in this context in [12, 16]; preliminary results were obtained by Yoshino, but no systematic study had been performed.

The Sinai model is an example of a one-dimensional self-similar potential with long-range correlations. In high dimensions, this problem is equivalent to a mean-field spin glass with a continuous replica symmetry breaking solution [43, 44]. In one dimension, however, there is no phase transition: the long-time, large-scale behaviour of the system is ruled by the zero-temperature fixed point, where the deepest minimum dominates. This is because the entropy in this model is of order one, whereas the energy scale increases as $\sqrt{L}$. However,

there are interesting static and dynamical crossover effects, as a function of the size of the system or of the time, that we study in detail in this paper. In particular, for finite waiting times, lowering the temperature leads to a localization effect which is a smeared version of the real localization transition that exists in the REM [9]. This kind of transition is known to bring about a large response against temperature changes [21], so that we expect to find rejuvenation effects in the dynamics of the Sinai model. Nevertheless, since time/length separation is not very drastic in the Sinai model, we find that rejuvenation and memory effects are present *in embryo*.

This paper is organized as follows. In the next section we present the Sinai model. In section 3 we analyse the statics of the model. In section 4 we discuss the dynamics, first by studying aging in the correlation length and then by studying the ac susceptibility during temperature cycles. In section 5 we give the conclusion derived from our analysis.

2. The model: Sinai potential

The Sinai model belongs to a wider class of random potential models. It describes the dynamics of a point particle under the action of a random, uncorrelated force field $F(x)$ which models several physical situations [39], such as the motion of a domain wall in the random field Ising model [45], or the motion of a dislocation kink. More recently, this model was argued to be relevant to describe some tapping experiments in sandpiles [46] and the unzipping transition of DNA [47]. The effective potential acting on the end point of the disordered directed polymer in 1 + 1 dimensions is also of the Sinai type [48–50]. However, in this case, the effective potential itself becomes temperature dependent, and the role of temperature changes in the directed polymer is much more subtle [24–26].

In the following, we will study the discrete Sinai model. The system consists of a box of length L in which we generate a random potential. Each sample of the random potential is constructed as follows. With each site of the box $i \in [1, L]$ we associate an independent random force f_i that is chosen according to a probability distribution which is Gaussian with zero mean, $\overline{f_i} = 0$, and variance $\overline{f_i f_j} = \sigma^2 \delta_{i,j}$. The potential in each site corresponds to the sum of the forces in the previous sites $V_i = -\sum_{j=1,i} f_j$, and is thus a *random walk* as a function of the position, i. Therefore, in this model each site corresponds to a different state or configuration with energy V_i, whose correlations (or barriers) increase as

$$\overline{(V_i - V_j)^2} = \sigma^2 |i - j|. \tag{1}$$

The partition function of this model at temperature T is defined by $\mathcal{Z} = \sum_i \exp(-V_i/T)$. This quantity has been much studied. It is known that the model has no thermodynamic transition so that in the limit $L \to \infty$, the physics is dominated by the $T = 0$ glassy fixed point [51–53]. As is obvious from equation (1), a rescaling in the length by a factor b is equivalent to a change in the scale of the potential by a factor $\sqrt{b}$, or of the temperature by a factor $1/\sqrt{b}$. As far as the statics is concerned, this means that being at low temperature in a small system is equivalent to having a larger system but at a higher temperature. For the dynamics a change in temperature leads to both a change in length scales and time scales.

3. Static chaos

3.1. Observables

Our aim is to investigate how the thermodynamic properties of the Sinai model change when comparing the same system at two different temperatures. In order to probe the change in

the free-energy landscape we have studied two different quantities, (i) the correlation function of the free-energy fluctuations at different temperatures and (ii) the correlation of the particle position. More precisely, we have studied the following observables:

- Free-energy correlations: we measure the free-energy fluctuations of the system at different temperatures averaged over the disorder

$$C_F(L, T_1, T_2) = \frac{\overline{\Phi_{T_1}\Phi_{T_2}}}{\sqrt{\overline{\Phi_{T_1}^2}}\sqrt{\overline{\Phi_{T_2}^2}}} \qquad \Phi_T \equiv F_T - \overline{F_T} \tag{2}$$

  where F_T is the free energy at temperature T and $\overline{(\cdot\cdot)}$ stands for the average over different disorder realizations of the potential. This quantity was originally proposed by Fisher and Huse [24] to study temperature chaos in the directed polymer problem. The fact that this correlation tends to zero with the size of the system shows that different energy valleys contribute to the total free energy at different temperatures. More recently, this quantity has been used to study the chaotic properties in the REM [21], and in the directed polymer problem when different types of perturbations are introduced [25], or for directed polymers on a hierarchical lattice [26].
- Fluctuations of position: a more geometrical way of visualizing 'temperature chaos' which could be of direct interest in some cases, for example the zipping and unzipping problem of DNA [47], is to consider the following quantity. With each site i, we associate a position $x_i = i/L$ and compute

$$d_{1,2} \equiv \overline{(\langle x\rangle_{T_1} - \langle x\rangle_{T_2})^2} \tag{3}$$

  where $\langle\cdot\cdot\rangle_T$ is the thermal average at temperature T, and $\overline{(\cdots)}$ is the disorder average. The study of the distance between average positions corresponding to different temperatures gives us an indication of the distance between states contributing to the partition function $\mathcal{Z}$ at different temperatures. If typical states contributing to $\mathcal{Z}$ at T_1 and T_2 are completely different, then $d_{1,2}$ will remain finite as $L \to \infty$. Note that $d_{1,2}$ has an upper bound $d_{1,2} \leqslant 1/6$, where $1/6$ is the value reached if the occupied sites are completely uncorrelated.

Both quantities C_F and d have been studied in the REM [21] to show that even if the energy landscape is fixed (in the sense that there is no reshuffling associated with the different valleys as temperature is changed), the model exhibits temperature chaos around the critical temperature, where the Boltzmann weight 'condenses' into a finite number of sites. Because there is no finite temperature transition in the Sinai model, one only observes mild effects under a temperature change, that are maximum around the crossover temperature $T \sim L^{1/2}$ (see below).

Numerically, we have investigated how these quantities behave as a function of L for different temperature differences. We have averaged over 2000 potential samples generated from Gaussian forces with zero mean and $\sigma = 1$. The sizes studied range from $L = 1$ to $L = 2^{14}$. The typical relative error for any of the observables is smaller than 0.1% so that error bars have not been included in the plots.

3.2. Thermodynamics of the model

The thermodynamics of the Sinai model has been well studied [51–53]. In the large L limit temperature is irrelevant. The system is frozen or localized in the minima of the potential, so that physical observables are governed by the ground state and its fluctuations. The free energy increases as $\overline{F} \sim -\sqrt{L}$ independent of temperature and the entropy reaches an L-independent

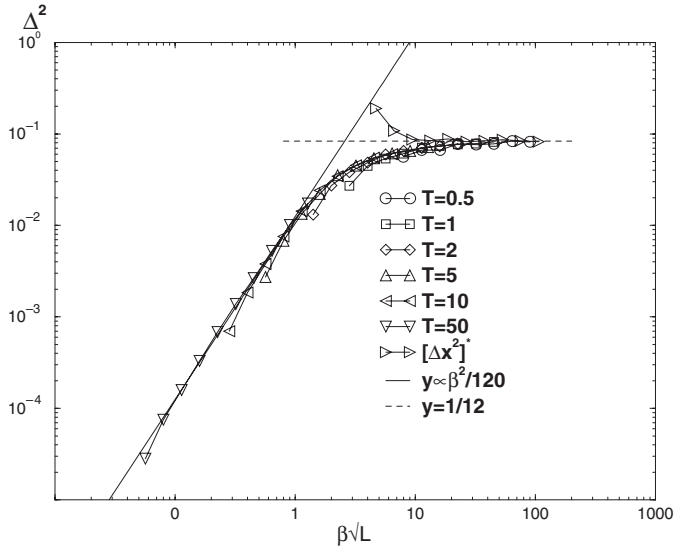

Figure 1. Sinai potential: Δ^2 plotted versus the scaling variable $g = \sigma\sqrt{L}/T$ for $T = 1, 2, 10, 50$ and 100. The dashed line corresponds to the position fluctuations at zero temperature. For small g we have plotted the high-temperature prediction $g^2/120$.

value which depends on temperature $\overline{S} = A + 2\ln T$. The free-energy fluctuations are also essentially dominated by the fluctuations of the deepest valley at any temperature. Therefore, it is reasonable to expect that in the thermodynamic limit a change in temperature has no significant effect on physical observables since the ground-state properties are temperature independent.

The finite-size corrections to the thermodynamic behaviour enter through the variable $g = \sigma\sqrt{L}/T$. Corrections are important when $g \sim 1$, or $L \sim L^* = (T/\sigma)^2$, signalling the crossover between two different limits:

- $L \ll L^*$: energy differences among different sites are much smaller than the temperature, so that all the sites contribute to the partition function.
- $L \gg L^*$: energy differences and barriers among different sites are huge and the particle is localized; only a few sites within the deepest valley contribute significantly to the partition function.

This crossover is clearly observed in the behaviour of the fluctuations of the mean position (in units of L):

$$\Delta^2 = \overline{\langle x\rangle^2} - \overline{\langle x\rangle}^2. \tag{4}$$

In figure 1 we show the results for different temperatures versus the scaling variable g defined above. The small g behaviour can be computed using a high-temperature expansion of the partition function

$$\Delta^2 = \frac{g^2}{120} + \mathcal{O}(g^4). \tag{5}$$

As we can see in the figure, the behaviour for small g matches this prediction nicely. For large g the system is completely governed by the $T = 0$ behaviour, thus the average position fluctuations should approach the fluctuations of the ground-state position. In figure 1, we

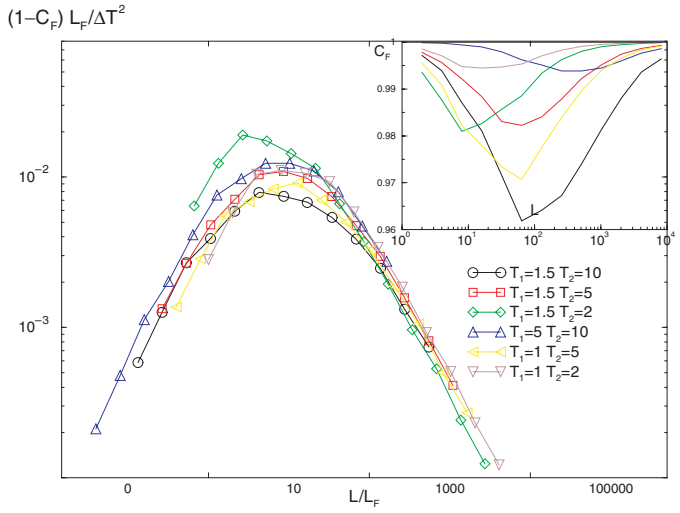

Figure 2. Scaling function for the free-energy correlations. $(1 - C_F) \times \frac{\sigma^2 L_F^*}{\Delta T^2}$ as a function of $\frac{L}{L_F^*}$ for different pairs of temperatures (T_1, T_2).

also plot the ground-state position fluctuations as a function of $\sqrt{L}$, that converges towards $1/12$. Numerically, we can see that this crossover takes place at $g \simeq 3$, corresponding to $L^* \simeq 10(T/\sigma)^2$.

This static crossover can be mapped to the dynamical crossover from a Brownian diffusive regime to an activated regime as we will see in the analysis of the correlation length in section 4.1.

3.2.1. Free-energy fluctuations. As we can see from the inset in figure 2, the free-energy correlations are a non-monotonic function of L.[3] For small L the free energy at different temperatures starts decorrelating but at a certain length, $L_F(T_1, T_2)$, C_F reaches a minimum. Then, it starts increasing again and reaches $C_F = 1$ when $L \to \infty$ regardless of the temperature difference (provided it is finite) as expected. One can distinguish between two different regimes:

- $L \ll L_F^*$
  For small system sizes/large enough temperatures the energy landscape is essentially flat, so that all the sites contribute to $\mathcal{Z}$. Therefore, in this regime a high-temperature expansion is expected to yield the correct behaviour of C_F. The result is the following:

$$1 - C_F \propto (\beta_1 - \beta_2)^2 \sigma^2 L \qquad (\Delta\beta\sigma\sqrt{L} \to 0) \tag{6}$$

  where $\beta \equiv 1/T$.
- $L \gg L_F^*$
  In this limit the system is governed by the ground state and its fluctuations, thus we expect that for $L \to \infty$ the correlation is perfect. However, when $g_{1,2} = \sigma\sqrt{L}/T_{1,2}$ is large but finite, the free-energy landscape decorrelates slightly. The behaviour in the large L limit can be understood by very simple arguments. Suppose that $T = (T_1 + T_2)/2$ is small,

[3] We have numerically checked that the energy correlations have the same behaviour.

and that the relative temperature change is also small: $\epsilon = (T_1 - T_2)/T \ll 1$. Using $\partial F/\partial T = -S(T)$, where $S(T)$ is the entropy at temperature T, one finds

$$\Delta F = F(T_2) - F(T_1) = \Delta T\, S(T) + \mathcal{O}(\epsilon^3) \qquad \Delta T = T_1 - T_2. \tag{7}$$

Note that this relation is also true for the fluctuating part Φ of F. Substituting (7) into the expression for C_F and expanding for small ϵ, we finally get

$$C_F \approx 1 - \Delta T^2 \frac{\overline{S^2} - \overline{S}^2}{2\overline{\Phi^2}}. \tag{8}$$

We show in appendix A that the entropy fluctuations tend to a numerical constant K that we compute in the large L limit. Thus recalling that free-energy fluctuations scale as $\overline{\Phi^2} = K'\sigma^2 L$, where K' can be computed from [52], we find the following scaling behaviour for $1 - C_F$:

$$\lim_{L\to\infty} 1 - C_F \longrightarrow \frac{K\,\Delta T^2}{K'\sigma^2 L}. \tag{9}$$

- Crossover
  The crossover between both regimes will take place at a certain length L_F^* such that $\Delta\beta\sigma\sqrt{L_F^*} \sim \Delta T/\sigma\sqrt{L_F^*}$, which yields $L_F^* \sim T_1T_2/\sigma^2$. The maximum of $1 - C_F$ actually occurs for $L_F^* \approx 10\,T_1T_2/\sigma^2$. This suggests the following scaling form for $1 - C_F$:

$$1 - C_F = \frac{\Delta T^2}{\sigma^2 L_F^*} f\left(\frac{L}{L_F^*}\right) \tag{10}$$

  with $f(x) \sim x$ for $x \to 0$ and $f(x) \sim 1/x$ for $x \to \infty$. The resulting scaling plot is shown in figure 2. This scaling is acceptable only when temperature differences are not too large, as one would expect.

3.2.2. Position fluctuations. In figure 3 we show the curves corresponding to the average distance shift $d_{1,2}$ defined by equation (3) above, for several temperature differences. Again we find that this quantity is a non-monotonic function of L. As a matter of fact, the behaviour of both $d_{1,2}$ and C_F is similar, and the same type of argument can be used for both quantities.

- $L \ll L_d^*$
  In figure 3 we can see that for large temperatures, $d_{1,2}$ increases with system size. This behaviour can be explained by looking at a high-temperature expansion. As shown in appendix B, we find in this regime $d_{1,2} \approx \frac{1}{120}(\Delta\beta)^2\sigma^2 L$.
- $L \gg L_d^*$
  In the large L region the behaviour of $d_{1,2}$ should be governed by the ground-state fluctuations. One starts from the relation

$$\langle x\rangle_{T_1} - \langle x\rangle_{T_2} = \frac{\epsilon}{T}\left(\langle x V_x\rangle_T - \langle x\rangle_T\langle V_x\rangle_T\right) \qquad \epsilon = \frac{\Delta T}{T} \tag{11}$$

  where $\langle\cdots\rangle_T$ is the thermal average at temperature T. This relation is derived from the fluctuation–dissipation relation ($\partial\langle x\rangle/\partial\beta = -\langle x V_x\rangle_c$) and integrating it assuming $\epsilon \ll 1$. The main contribution to $d_{1,2}$ for small temperatures will come from two nearly degenerate valleys that are a distance $\sim L$ apart. Restricting the thermal averages to these two valleys, one finds

$$\langle x\rangle_{T_2} - \langle x\rangle_{T_1} \approx \frac{\epsilon}{T} D\sigma\eta\sqrt{L}\,\mathrm{e}^{-\beta\sigma\eta\sqrt{L}} \tag{12}$$

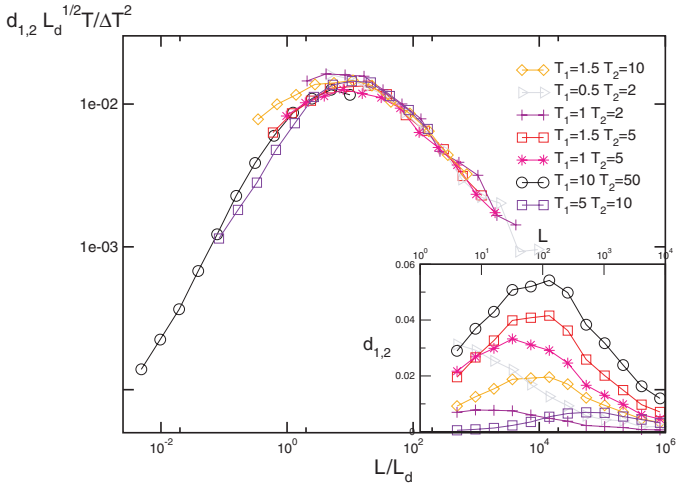

Figure 3. Rescaled average distance shift $d_{1,2} \times \frac{(T_1T_2T)^{\frac{2}{3}}}{(\Delta T)^2}$ plotted versus L/L_d^* for different T_1 and T_2.

where D is the distance between the two valleys, and $\sigma\eta\sqrt{L}$ is their energy difference, such that η is a positive random variable of order unity. In order to obtain $d_{1,2}$ we have to compute $\overline{(\langle x_2\rangle - \langle x_1\rangle)^2}$. This average depends on the joint probability distribution of the excitations $P(\eta, D)$. It is reasonable to assume that the probability distribution factorizes as $P(\eta, D) = h(\eta)p(D)$. Therefore in the limit $\beta\sigma\sqrt{L} \to \infty$ we have

$$\overline{D^2\eta^2\,\mathrm{e}^{-2\beta\eta\sqrt{L}}} = \overline{D^2}\int_0^\infty \mathrm{d}\eta\, h(\eta)\,\mathrm{e}^{-2\beta\sigma\eta\sqrt{L}}\eta^2 \sim \overline{D^2}\frac{h(0)}{(\beta\sigma)^3L^{3/2}}. \tag{13}$$

Recalling that x is the rescaled distance i/L, one expects $\overline{D^2} \sim 1$. Provided $h(0) \neq 0$, one finally finds

$$d_{1,2} \sim \frac{\Delta T^2}{T\sigma\sqrt{L}} \qquad (\beta\sigma\sqrt{L} \to \infty). \tag{14}$$

- Crossover

  As for the free-energy correlation, we can extract a crossover length scale which separates both regimes. The crossover length that is obtained is $L_d^* \sim (T_1T_2)^{\frac{4}{3}}T^{-\frac{2}{3}}$, that coincides with L_F^* in the limit $T_1 = T_2$. Again, we can try a scaling formula

$$d_{12} = \frac{(\Delta T)^2}{(T_1T_2T)^{\frac{2}{3}}}h\left(\frac{L}{L_d^*}\right) \qquad \text{where} \quad \begin{cases} h(x) \sim x & x \to 0 \\ h(x) \sim \frac{1}{\sqrt{x}} & x \to \infty. \end{cases} \tag{15}$$

  Note that the functions f and h are quite different. This reflects the fact that the two observables probe different mechanisms. In figure 3 we show the scaling plot for different pairs (T_1, T_2). Note that *all* the curves display the maximum at the same value of the scaling variable $\frac{L}{L_d^*} \simeq 10$.

3.3. Discussion

The outcome of the numerical analysis of the Sinai potential is clear: in the thermodynamic limit statistical properties are governed by the $T = 0$ fixed point. This means that, regardless of temperature, for large enough system sizes, the system only sees the free-energy valley associated with the global minimum. Effectively this situation is equivalent to saying that in this limit there is no chaos in temperature since the statistical properties are those of the minimum of the potential.

This situation is very different from what happens in the directed polymer problem. This model, as well as the Sinai model, has no thermodynamic transition. It only displays a low-temperature glassy phase. In a recent paper [25], this model has been shown to be extremely sensitive to any perturbation leading to the vanishing of correlations between systems at different temperatures (see also [26, 34] for a related discussion). In this model this is due to the existence of anomalous large excitations which have a very low free-energy cost. These excitations cost a lot of energy, and hence energy fluctuations are large $\sqrt{\overline{(\Delta E)^2}} \sim L^{1/2}$, but are very favoured entropically, $T\sqrt{\overline{(\Delta S)^2}} \sim L^{1/2}$, so that these two contributions may cancel to yield a lower cost in free energy $\sim L^{1/3}$. In the Sinai model these anomalous excitations do not exist because the entropy is very small (not extensive) and never cancels the energy cost ($\sim L^{1/2}$) of such excitations.

It is interesting to compare the above crossover lengths $L^*_{d,F}$ with the crossover length at each temperature $L^*_T \sim (T/\sigma)^2$. The maximum decorrelation takes place for a system size such that $L^*_2 < L = L^*_{d,F} < L^*_1$. In this case the system at T_2 is already localized whereas the system at T_1 is still delocalized. The strong influence of temperature shift in this case is a smeared out version of the infinite susceptibility found in the random energy model [21]. In the latter there is a true finite temperature phase transition, and not a mere crossover as in the Sinai case. For larger system sizes, when $L^*_1 < L^*_2 < L$, both systems are governed by the zero-temperature fixed point and correlations increase.

4. Dynamics

The dynamics of this model have been well studied, both analytically [38, 41] and numerically [40]. Single-time as well as two-time quantities have been analysed. Here, we study one observable of both types; we define in particular an 'ac susceptibility' that should be closely related to the analogous observable studied in spin glasses.

In our simulations we have used boxes of length $L = 1024$ with periodic boundary conditions. The dynamics has been simulated by the Monte Carlo method using the Metropolis algorithm. For each realization of the random potential, in order to sample adequately the energy landscape we have considered all possible initial conditions ($L = 1024$) and have averaged over $n \sim 100$ different histories for each starting point. The total number of samples used in temperature cycling experiments is around 200–300. Despite the low number of samples used, the average over many different thermal histories ($100 \times L$) for each sample is enough to ensure small sample-to-sample fluctuations of dynamical quantities. Typical error bars are of around 0.5% for high temperatures but much smaller ($\approx$0.05%) for the lowest temperatures simulated ($T = 0.1, 0.2, 0.5$), so they have not been included in the plots.

We have analysed two different quantities:

- The correlation (or explored) length:

$$\xi^2(t) = \overline{\langle (x(t) - x(0))^2 \rangle}. \tag{16}$$

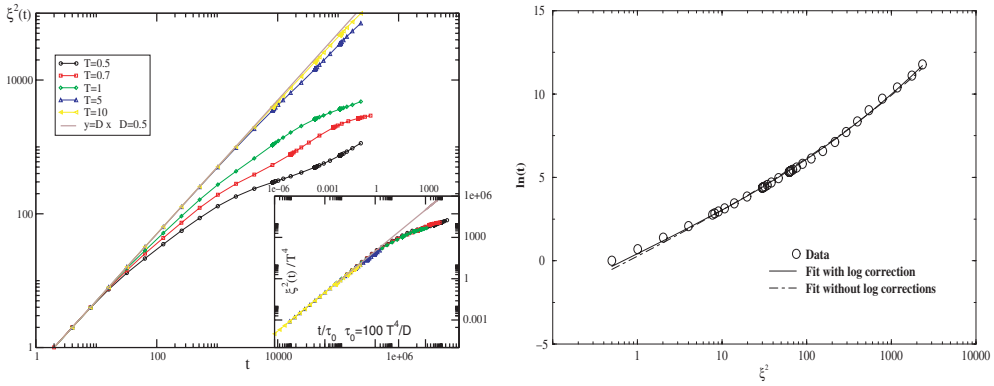

Figure 4. Left: correlation length versus time for different temperatures. The solid line corresponds to the short-time diffusive behaviour $\xi(t) \sim \sqrt{t}$. In the inset we plot ξ^2/T^4 versus the scaling variable $\tau = t/200T^4$. Averages over 75×1024 histories. Right: $\ln t$ versus ξ^2 for $T = 0.7$ fitted with the effective function in (19), with and without the $\ln\ln\ell$ correction.

The brackets and overline mean that we average over both the $L \times n$ histories and samples respectively. The initial condition is a uniform distribution equivalent to a quench from infinite temperatures. This correlation length only gives information about the 'large-scale' mechanisms and the temperature cycling effects on this quantity can be fully explained in terms of effective times.

- In order to probe 'smaller' length scales that are more sensitive to temperature changes, we have defined the following 'ac' susceptibility $\chi(\omega, t_w)$:

$$\chi(\omega, t_w) \equiv \overline{\left\langle \left(x\left(t_w + \frac{1}{\omega}\right) - x(t_w)\right)^2 \right\rangle}\Bigg|_{\mathcal{P}(x,t_w)} \tag{17}$$

where the average is taken over the probability $\mathcal{P}(x, t_w)$ that a particle is at position x at time t_w, starting from a uniform distribution of particles at time $t = 0$.[4] In other words, we measure the typical extra distance travelled by particles in a time $1/\omega$, weighted by the dynamical distribution at time t_w. Such a quantity was also considered in [40, 41].

Our main interest in this section is to study the temperature cycling experiments which are carried out in spin glasses that have shown striking rejuvenation and memory effects [16, 17]. Our main goal here is to see to what extent these effects are already present in the Sinai model. We have performed numerically the standard temperature cycling experiment: quench from infinite temperature down to T_1 and let the system relax during t_{w_1}; then change the temperature to $T_2 = T_1 + \Delta T$ and let the system evolve during t_{w_2} and finally return to T_1. We have studied cycles with positive and negative ΔT for several waiting times and frequencies.

4.1. The correlation length

The time evolution for the correlation length at different temperatures is shown in the left-hand panel in figure 4. The growth of the correlation length depends exclusively on a temperature-dependent microscopic time scale $\tau_0(T)$. This time scale is related to the crossover between two different dynamical regimes [38, 41]:

[4] We have also investigated the case where the initial distribution is localized on an arbitrary point, with similar results.

- $t \ll \tau_0$: short-time dynamics where no barriers are present, so that in this regime we have the usual Brownian diffusion $\xi^2(t) = Dt$.
- $t \gg \tau_0$: long-time, activated dynamics, with an activation time which follows an Arrhenius law with a typical barrier $B \sim \sigma\sqrt{L}$ [38]. Using $t = \tau_0 \, \mathrm{e}^{B/T}$ and $L \sim \xi$ leads to $\xi^2(t) \sim (T/\sigma)^4 \ln^4\left(\frac{t}{\tau_0}\right)$.

The crossover takes place when barriers become comparable to temperature so that activation between valleys dominates the dynamics. This crossover is directly related to the static crossover found for position or free-energy correlations from a high-temperature regime (no barriers) to a (thermodynamic) low-temperature regime (see section 3.2). The microscopic time scale can thus be identified with the time that typically the system takes to explore this static crossover length scale $L^* \simeq 100(T/\sigma)^2$. Therefore, for $\sigma = 1$, $\tau_0(T) = L^{*2}/D \simeq 200T^4$ (D can be evaluated to be $D \approx 0.5$).

One, therefore, expects that the correlation length at a given temperature (16) can be expressed as $T^4 f(\tau)$, where f is a function of the scaling variable $\tau = t/\tau_0$, with

$$\begin{cases} \tau \ll 1 & f(\tau) \sim \tau \\ \tau \gg \tau_0(T) & f(\tau) \sim \ln^4 \tau. \end{cases} \tag{18}$$

This scaling behaviour works very well, as shown in the inset of figure 4, where we rescale together all temperatures. Such a crossover between a short-time growth law and a long-time activated behaviour is also expected in the droplet description of spin glasses [14, 17, 19, 54], or directed polymers, where barriers grow with the size ℓ of the excitations as $B(\ell) = \Upsilon \ell^{\psi}$, where Υ is a function of temperature. This leads to a logarithmic growth of the size of the droplets, $\ell \sim \left(\ln \frac{t}{\tau_0}\right)^{\frac{1}{\psi}}$, where τ_0 is a microscopic attempt time, possibly renormalized by critical fluctuations [17, 55, 56]. The Sinai case corresponds to $\psi = 1/2$ and $\tau_0 \propto \ell^2$. As a more precise description of the crossover, we have shown in figure 4 the following fit:

$$t(\ell) = A\ell^2 \exp(B\sqrt{\ell \ln \ln \ell}) \tag{19}$$

where the $\ln \ln \ell$ accounts for the famous Khinchin iterated logarithm law for the maximum of a random walk [57]. Note that the two kinds of limiting behaviour for ξ^2 in (18) are consistent with this last expression. In figure 4 the right-hand plot shows $\ln t$ versus ξ^2 for $T = 0.7$ which are nicely fitted by the expression above.

The correlation length is a monotonic function of time and temperature. The temperature only plays the role of slowing down dynamics, therefore a change in temperature only changes the growth law. Any time t_w spent at a temperature T_1 is equivalent to having spent an effective time $t_{\mathrm{eff}}(t_w, T_1, T_2)$ at T_2 such that $\xi^2(t_w, T_1) = \xi^2(t_{\mathrm{eff}}, T_2)$. Thus in temperature cycling protocols there is no trace of the chaotic effects observed experimentally on the correlation length itself (see figure 5).

4.2. Susceptibility

In the previous section we have studied the correlation length $\xi(t_w)$ that tells us how far the particle can go in a time t_w. This quantity is the analogue of the size of the domains in a droplet coarsening description. However, in ac experiments after a negative temperature shift one probably observes how the 'domain walls' reconform on a scale which is small compared to $\xi(t_w)$. The susceptibility defined in (17) probes these 'small' length scales and might show an interesting behaviour during temperature cycling, not revealed by $\xi(t_w)$ (see figure 5). The study of the 'response' function (17) is useful because the results admit an intuitive interpretation in terms of the evolution of $\mathcal{P}(x, t_w)$, which is the quantity that keeps track of the thermal history of the system.

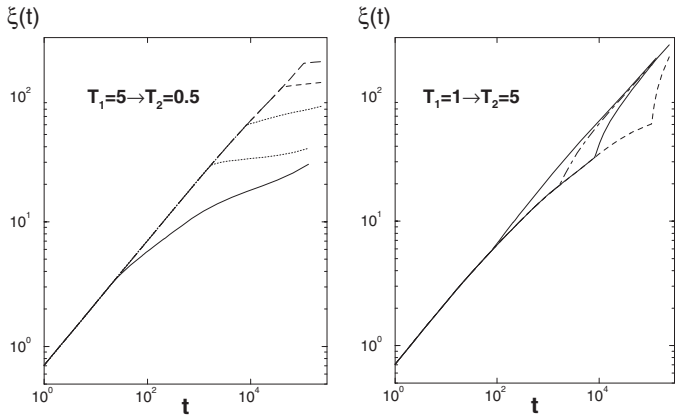

Figure 5. Correlation length $\xi(t)$ versus time for the following experiments. Left: spend t_w at $T_1 = 5$ and then quench the system down to $T_2 = 0.5$ for $t_w = 16, 1662, 8192, 40\,959$ and $106\,494$ from bottom to top. Right: spend t_w at $T_1 = 1$ and then heat the system up to $T_2 = 5$ for $t_w = 79, 1662, 8192$ and $106\,494$.

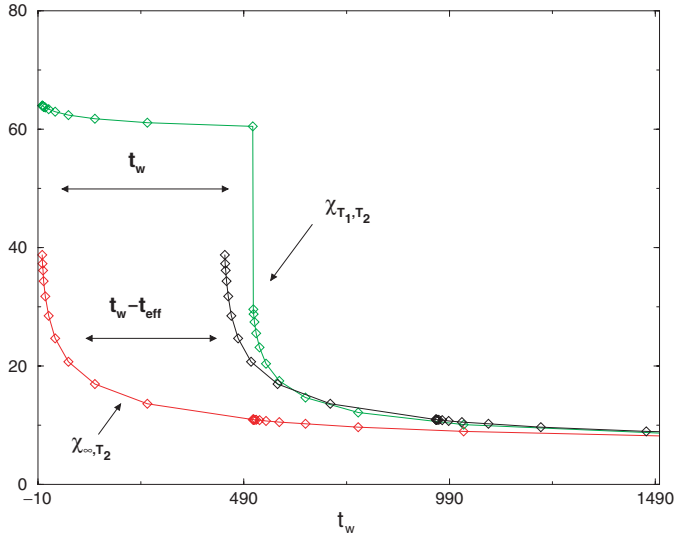

Figure 6. Measure of the effective time when cooling the system down to $T_2 = 0.5$ after having spent $t_{w1} = 512$ at $T_1 = 5$ at $\omega = 1/128$. Note that only the late part of the curves can be superimposed: there is a transient that cannot be accounted for using an effective time.

In order to compare with experiments, one should have the following conditions: long waiting times t_w and low frequencies ω, but such that $\omega t_w \gg 1$. This last condition is imposed by the fact that a harmonic response can only be measured on a time larger than one oscillation period. This also ensures that one is in a regime where the violations of the fluctuation–dissipation theorem are weak and one can identify the fluctuation that we measure, (17), to a *response* [12].

From the results of the simulations we observe that the effect of aging at temperature T_1 on the relaxation at T_2 strongly depends on the temperature difference and on the waiting time. This effect can be quantified by defining an effective time (figure 6). For instance, when

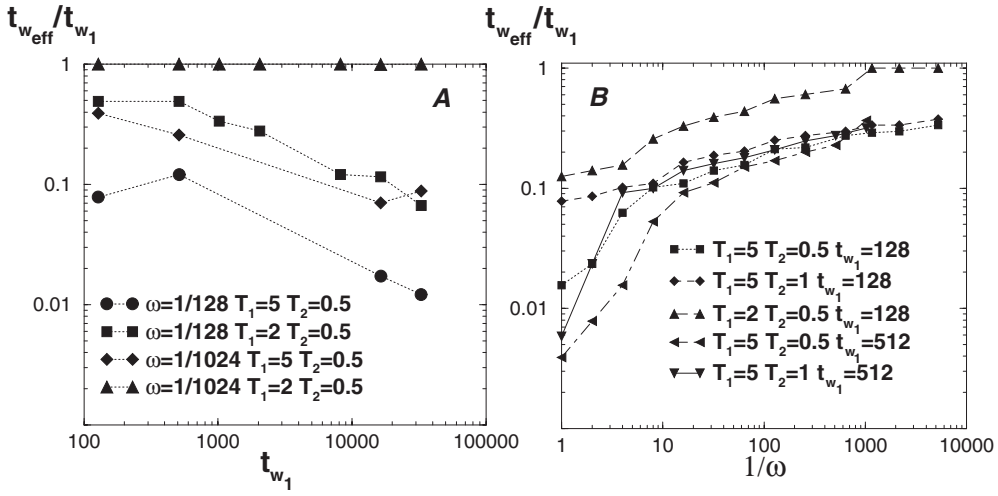

Figure 7. Normalized effective times $t_{\rm eff}/t_{w_1}$: (A) at fixed ω versus t_{w1}, (B) at fixed t_{w1} versus $1/\omega$.

cooling the system from T_1 to T_2 one expects that if the system is completely rejuvenated, the relaxation curve $\chi_{T_1,T_2}(\omega, t_{w2})$ should correspond to that obtained after quenching from high temperature $\chi_{\infty,T_2}(\omega, t_{w2})$. (Here t_{w2} is counted from the time at which the system reaches T_2.) However, if the relaxation at T_1 affects aging at T_2 then rejuvenation is only partial and the new relaxation corresponds to that of the system after aging during an effective time $t_{\rm eff}$ at T_2, $\chi_{\infty,T_2}(\omega, t_{w2} + t_{\rm eff})$. Thus if $t_{\rm eff} = 0$, rejuvenation is complete. In figure 7 we show how this effective time is measured. Note that only the late part of the curves can be superimposed: there is a transient that cannot be accounted for using an effective time. A similar effect can be observed in spin glasses. The same effective time can also be defined when heating back the system, as a measure of memory recovery.

Experimentally, the observed facts in spin glasses are the following:

- When cooling the sample from $T_1 < T_c$ to $T_2 < T_1$, $t_{\rm eff}$ is larger than t_{w1} when ΔT is small enough, indicating that aging at T_1 is more efficient because it is faster at higher temperature [58]. However, as ΔT increases, $t_{\rm eff}$ starts decreasing towards zero. In other words, for large enough ΔT, *rejuvenation* is complete. A related phenomenon is the absence of cooling rate effects. The relaxation at low temperature does not depend on the cooling history. Only the very last steps at nearby temperatures determine the final relaxation [12].
- When heating back from T_2 to T_1 the system resumes its relaxation, for large enough ΔT, as if the stay at lower temperatures did not take place (perfect *memory*). As ΔT is reduced, an effective age $<t_{w2}$ that accounts for the time spent at T_2 must be added. Furthermore, a small transient appears at short times, this was called 'memory anomaly' in [58]. As in experiments, this anomaly is non-monotonic with ΔT: for small ΔT, the reference curve corresponding to perfect memory is reached from *below*, whereas for larger ΔT, it is reached from *above* [58]. Finally, for still larger ΔT, memory is perfect, as stated above.

  Note that if the time t_{w1} spent at T_1 at the first stage of the cycle is very small, one expects, from the previous discussion, to see 'rejuvenation' after heating back to T_1 in the negative temperature cycle, since the system has kept the memory of the age it had on the

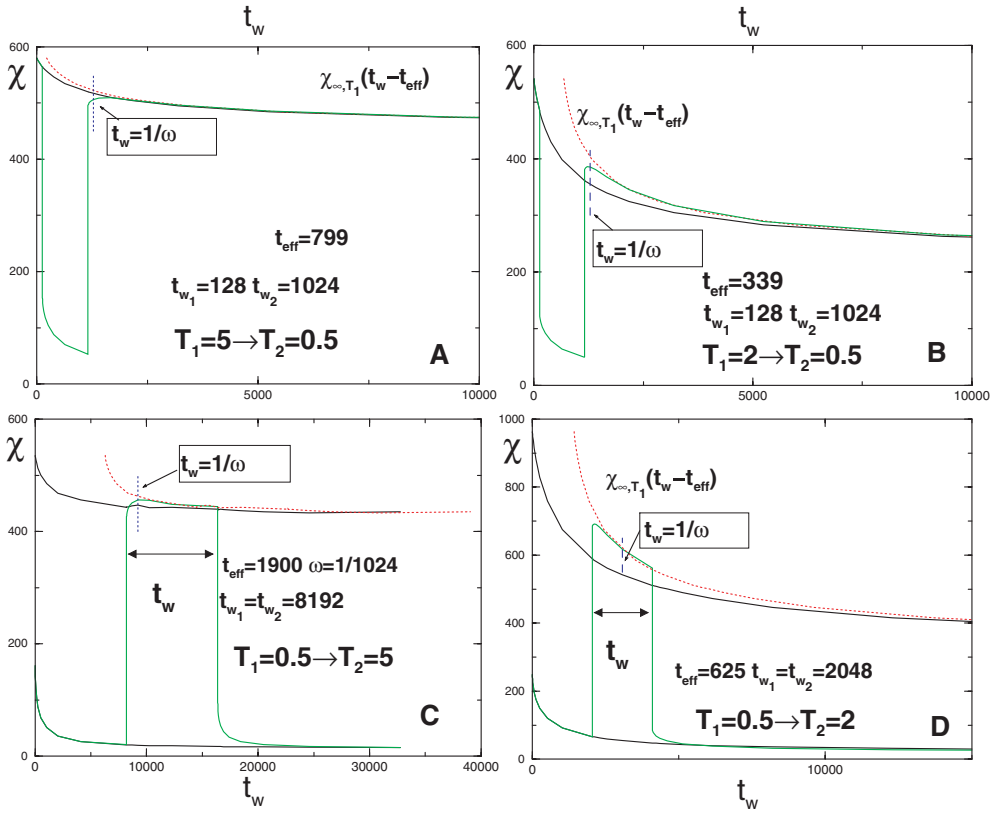

Figure 8. Negative and positive temperature cycles. (A) and (B) correspond to cycles with $\Delta T < 0$, data for $\omega = 1/128, t_{w_1} = 128, t_{w_2} = 1024$ and for cycle (A): $T_1 = 5, T_2 = 0.5$ and (B): $T_1 = 2, T_2 = 0.5$. (C) and (D) correspond to cycles with $\Delta T > 0$, for cycle (C): $T_1 = 0.5, T_2 = 5, \omega = 1/1024$ and $t_{w_1} = t_{w2} = 8192$ and (D): $T_1 = 0.5, T_2 = 2, \omega = 1/1024$ and $t_{w_1} = t_{w2} = 2048$. The dashed line corresponds to the first measurement possible in a regular experiment $t_w = 1/\omega$.

way down, i.e. $t_{w1} \ll t_{w2}$. This rejuvenation after a positive ΔT has been observed many times experimentally.

Let us now turn to the results of the simulations, following the above presentation of experimental data.

- The data of figure 8 correspond to temperature cycles with $T_1 = 5, T_2 = 0.5$ or $T_1 = 2, T_2 = 0.5$. The main observation here is that clear rejuvenation is observed, with an effective shift time that decreases as ΔT increases, as in the experiments. Intuitively, this corresponds to the fact that since the potential is self-similar, the *local* dynamics probed by $\chi(\omega, t_w)$ is not sensitive to the depth of the potential valley that is currently occupied. Therefore, aging at T_1 has already selected some low-lying valleys, but the intra-valley dynamics is insensitive to this. This argument for rejuvenation based on a hierarchical energy landscape, and in the absence of temperature chaos has been put forward in [6, 7, 16, 17], and has been confirmed numerically in the multi-level trap model in [22]. In figure 7 we show the normalized effective waiting times as a function of both t_{w1} and $1/\omega$. Note that lower frequencies, that correspond to larger length scales, are less

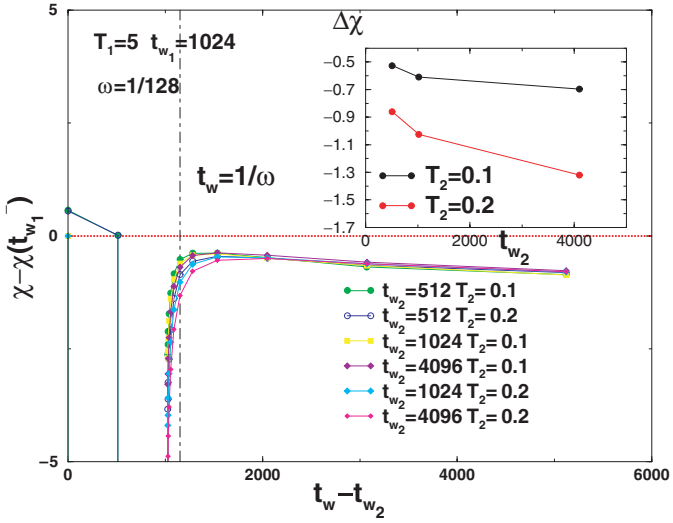

Figure 9. Memory anomaly in a negative temperature cycle at fixed ω. We plot the $\chi - \chi(t_{w_1}^-)$ at fixed $\omega = 1/128$ and $t_{w_1} = 1024$ for the temperature changes $T_1 = 5$, $T_2 = 0.1, 0.2$ for different $t_{w_2} = 512, 1024, 4096$. In the inset we plot $\Delta\chi$ as defined in (20) for the different t_{w2}.

easily rejuvenated, as expected, since the separation of time scales is not as sharp (see the triangles in figure 7).

- When heating the system back to the initial temperature T_1, some memory is observed. However, (i) when the temperature difference is not very large, some effective time, accounting for the period spent at T_2, must be included, as in the experiments, and (ii) a strong transient 'memory anomaly' is observed, even for quite large ΔT (see (A) and (B) in figure 8). The memory anomaly is defined as

$$\Delta\chi = \chi(t_{w1} + t_{w2} + 1/\omega) - \chi(t_{w1}^-) \tag{20}$$

where $\chi(t_w = t_{w1}^-)$ is the susceptibility just before the quench and $\chi(t_{w1} + t_{w2} + 1/\omega)$ corresponds to the first possible measurement at frequency ω after heating back to T_1. In figures 9 and 10 the dependence of the memory anomaly on different parameters, including the frequency, is shown. Note that we have always observed this memory anomaly to be negative, i.e. the reference curve is reached from below.

In figure 9 we show how the memory anomaly varies with the time t_{w2} spent at T_2, for a fixed $\omega = 1/128$ and $t_{w1} = 1024$, for the largest ΔT. From the inset, we see that the larger ΔT, the smaller $|\Delta\chi|$, which agrees with the interpretation that the strong rejuvenation effect found for large ΔT arises from the separation of length scales. In the plot in figure 10 we show how the memory anomaly depends on the frequency ω. Since the susceptibility at t_{w1} itself depends on ω we plot the relative variation of the susceptibility with respect to $\chi(t_{w1}^-)$ at fixed $t_{w1} = t_{w2} = 1024$. In the inset we show $\Delta\chi/\chi(t_{w1}^-)$ versus ω. Note that $\Delta\chi/\chi(t_{w1})$ is always negative and its absolute value decreases with increasing $1/\omega$. In [58], Sasaki *et al* find that the anomaly can be both positive and negative when one works in the vicinity of a transition temperature. In the Sinai model we have not been able to observe such a positive anomaly. For smaller ΔT these effects are blurred because length scale separation becomes weak. Aging at different temperatures is cumulative and $\Delta\chi/\chi$ is also larger (see figure 8 for the $T_1 = 2 \to T_2 = 0.5$ cycle). For these smaller ΔT, we have found that the memory anomaly becomes non-monotonic with frequency.

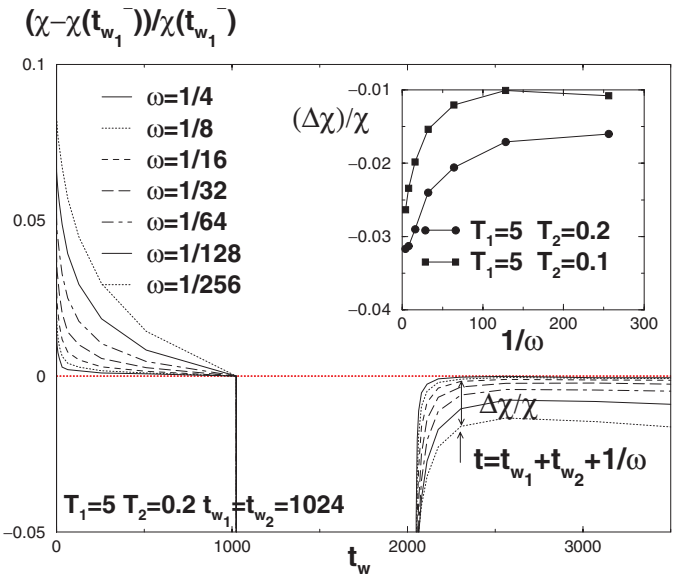

Figure 10. Memory anomaly in a negative temperature cycle at fixed ΔT. $\Delta\chi/\chi(t_{w1}^-)$ for the cycle $T_1 = 5$, $T_2 = 0.2$ with $t_{w1} = t_{w2} = 1024$ we plot $\Delta\chi/\chi(t_{w1}^-)$ for different frequencies, $\omega = 1/4, \ldots, 1/256$. In the inset we plot $\Delta\chi/\chi$ versus $1/\omega$ for this case and for the cycle $T_1 = 5$, $T_2 = 0.1$ with the same parameters.

- Positive temperature cycle experiments. We have also observed that the third stage is completely independent of t_{w1}. Heating the system back to T_2 erases the initial aging accumulated at T_1. This is expected, since the dynamics at T_2 allows the system to leave the traps that it had slowly explored at T_1. The new relaxation at T_1 is aged, but the age is only due to the effect of aging at T_2. This is similar to the effect observed experimentally.

5. Discussion

In this paper we studied in detail the role of temperature shifts in the simplest model where the energy landscape is explicitly hierarchical, namely the Sinai model. This model has both attractive features (there are valleys within valleys in a strict self-similar sense), but also one important drawback: there is no phase transition so that the model, in the large-size limit, is effectively at zero temperature. Therefore, in this limit, temperature shifts do not lead to interesting phenomena: entropy in this model does not play any role, so that excitations have an enormous free-energy cost and cannot be favoured by the temperature perturbation, contrarily to what happens in a closely related model, the directed polymer [25] (see also [34]).

Nevertheless, for finite sizes/finite times, some interesting crossover phenomena qualitatively reproduce the spin-glass phenomenology. In particular, dynamical rejuvenation effects in the absence of temperature chaos are observed. This rejuvenation is ascribed to the local dynamics, which is insensitive (due to the self-similar nature of the potential) to the particular valley that has been reached during aging at a higher temperature. Still, the separation of time scales/length scales with temperatures is much weaker than in experimental spin glasses [17], partly due to the rather modest time scales investigated in the present study.

Correspondingly, abrupt rejuvenation as the temperature is decreased and strict memory when the temperature is cycled cannot be achieved. Rejuvenation and memory are present *in embryo*.

In other words, the Sinai model is a smeared out version of the multi-level trap model studied in [7, 22], where the sequence of critical temperatures is replaced by a gradual freezing in the detail of the fractal landscape. One could have studied the effect of temperature shifts in a one-dimensional potential with logarithmic correlations (rather than linear, as in the Sinai case). This model was studied in detail in [59] and was shown to exhibit a true transition temperature. We expect the resulting temperature shift phenomenology to be very close to that of the random energy model, explored in [21]. An extension of this model, that has an infinite sequence of phase transitions, will be presented in the near future [60].

Acknowledgments

We thank L Berthier, V Dupuis, O Martin, M Sasaki, E Vincent and H Yoshino for discussions. H Yoshino participated in an early stage of the project. MS thanks the MEC for grant AP98-36523875. FR wishes to thank the Ministerio de Ciencia y Tecnología in Spain, project BFM2001-3525 and Generalitat de Catalunya for financial support.

Appendix A. Calculation of the entropy fluctuations in the deepest well

In this appendix we compute the average entropy fluctuations of the Sinai model in the large L limit. As we have already said in section 3.2.1, these entropy fluctuations are constant in this limit. For this computation we only need to consider the contribution to the partition function arising from the deepest minima. In a recent paper [42], Monthus and Le Doussal compute the probability distribution of the partition function of the deepest well considering that the origin in energies is at the bottom of the potential. They compute $P(\mathcal{Z})$ obtaining the Laplace transform as

$$\int_0^\infty \mathrm{d}\mathcal{Z}\, \mathrm{e}^{-t\mathcal{Z}} P(\mathcal{Z}) = \frac{1}{I_0^2(a\sqrt{t})} \qquad a = \frac{2}{\beta\sigma} \tag{A.1}$$

where $\beta = 1/T$ and σ^2 is the variance of the random force. This result implies that we can work in terms of a dimensionless partition function $z = \mathcal{Z}/a^2$ to obtain

$$\int_0^\infty \mathrm{d}z\, \mathrm{e}^{-tz} p(z) = \frac{1}{I_0^2(\sqrt{t})}. \tag{A.2}$$

Since the energy of the absolute minimum is set to zero, the entropy fluctuations can be directly computed as

$$\overline{S(T)^2} - \left(\overline{S(T)}^2\right) = \overline{\ln^2 \mathcal{Z}} - \overline{\ln \mathcal{Z}}^2. \tag{A.3}$$

Now in terms of the dimensionless partition function we have that $\ln \mathcal{Z} = \ln z + \ln a^2$, thus when computing fluctuations of averages over z terms which depend on a (and thus on T) cancel to yield

$$\overline{S(T)^2} - \left(\overline{S(T)}^2\right) = \overline{\ln^2 z} - \overline{\ln z}^2 = \int_0^\infty \mathrm{d}z\, p(z)(\ln z)^2 - \left(\int_0^\infty \mathrm{d}z\, p(z) \ln z\right)^2 \tag{A.4}$$

which is a constant as we expected. This constant can be evaluated by computing the averages of $\ln z$ and $\ln^2 z$. The starting point of the calculation is Derrida's integral representation of the logarithm,

$$\ln \mathcal{Z} = \lim_{q\to 0} \int_q^\infty \mathrm{d}t \frac{1}{t}(\mathrm{e}^{-t} - \mathrm{e}^{-t\mathcal{Z}}). \tag{A.5}$$

When we perform the average of e^{-tz} we obtain the Laplace transform given in (A.2), thus

$$\overline{\ln z} = \lim_{q\to 0}\int_q^\infty dt\,\frac{1}{t}\left(\frac{1}{I_0^2(\sqrt{t})} - e^{-t}\right). \tag{A.6}$$

This integral can be split into two parts, the exponential integral

$$\int_q^\infty dt\,\frac{1}{t}e^{-t} = -\gamma - \ln q + q + \frac{q^2}{2} + \cdots \lim q \to 0 \tag{A.7}$$

where γ is the Euler constant, and the part with the Bessel function,

$$\int_q^\infty dt\,\frac{1}{t}\frac{1}{I_0^2(\sqrt{t})} = 2\int_{\sqrt{q}}^\infty dt\,\frac{1}{t}\frac{1}{I_0^2(t)} = 2\int_{\sqrt{q}}^\infty dt\left(-\frac{d}{dt}\frac{K_0(t)}{I_0(t)}\right) = 2\frac{K_0(\sqrt{q})}{I_0(\sqrt{q})}$$
$$= -\ln q + 2\ln 2 - 2\gamma + (\psi(2)-1)\frac{q}{8} + \cdots \tag{A.8}$$

where we have used the Wronskian property of the Bessel functions

$$-\frac{1}{t} = K_\nu'(t)I_\nu(t) - K_\nu(t)I_\nu'(t). \tag{A.9}$$

Adding these two contributions we obtain that the average entropy reads

$$\overline{S(T)} = \overline{\ln \mathcal{Z}} = -2\ln a - 2\ln 2 + \gamma. \tag{A.10}$$

To compute the average $\ln^2 z$ we have to evaluate the following integral:

$$\overline{\ln^2 z} = \lim_{q\to 0, p\to 0}\int_q^\infty dt\int_p^\infty dt'\,\frac{1}{tt'}\left(e^{-t-t'} - \frac{e^{-t'}}{I_0^2(\sqrt{t})} - \frac{e^{-t}}{I_0^2(\sqrt{t'})} + \frac{1}{I_0^2(\sqrt{t+t'})}\right). \tag{A.11}$$

The contribution arising from the first three terms in the integral can be evaluated from expressions (A.6) and (A.7) to obtain

$$\int_q^\infty dt\int_p^\infty dt'\frac{e^{-t-t'}}{tt'} = \gamma^2 + \gamma\ln qp + \ln q\ln p + \mathcal{O}(q,p)$$
$$\int_q^\infty dt\int_p^\infty dt'\frac{e^{-t}}{tt'}\frac{1}{I_0^2(\sqrt{t'})} = (\gamma + \ln q)(2\gamma - 2\ln 2 + \ln p) \tag{A.12}$$
$$\int_q^\infty dt\int_p^\infty dt'\frac{e^{-t'}}{tt'}\frac{1}{I_0^2(\sqrt{t})} = (\gamma + \ln p)(2\gamma - 2\ln 2 + \ln q).$$

The last term is somewhat more involved and can be evaluated as follows:

$$\int_q^\infty dt\int_p^\infty dt'\frac{1}{I_0^2(\sqrt{t+t'})} = 2\int_q^\infty dt\,\frac{1}{t}\frac{K_0(\sqrt{t+p})}{I_0(\sqrt{t+p})} + 2\int_p^\infty dt'\,\frac{1}{t'}\frac{K_0(\sqrt{t'+q})}{I_0(\sqrt{t'+q})}. \tag{A.13}$$

In the limit $p \to 0$ the integral can be Taylor expanded yielding

$$\int_q^\infty dt\,\frac{1}{t}\frac{K_0(\sqrt{t+p})}{I_0(\sqrt{t+p})} = \int_q^\infty dt\,\frac{1}{t}\frac{K_0(\sqrt{t})}{I_0(\sqrt{t})} + \mathcal{O}(p) \tag{A.14}$$

where the terms of order p do not contribute when we set p to 0. Hence we can evaluate expression (A.13) at $p = 0$ to obtain

$$\int_q^\infty dt\,\frac{1}{t}\frac{K_0(\sqrt{t})}{I_0(\sqrt{t})} = \frac{1}{2}\ln^2 q - 2\ln 2\ln q + 2\gamma\ln q + 2 \qquad \zeta = 0.2415\ldots. \tag{A.15}$$

Adding all the contributions and taking the double limit $q \to 0$ and $p \to 0$ we obtain the following result for $\overline{\ln^2 z}$:

$$\overline{\ln^2 z} = 4\zeta - 3\gamma + 4\gamma\ln 2 \tag{A.16}$$

which finally yields the entropy fluctuation

$$K = \overline{S^2} - \overline{S}^2 = 4(\zeta - (\gamma - \ln 2)^2) = 0.912\,784\ldots. \tag{A.17}$$

Appendix B. High-temperature expansion of the distance shift

We want to compute the high-temperature behaviour of the average distance shift between systems at two different temperatures $d_{1,2}$ as defined in equation (3),

$$\overline{(\langle x\rangle_1 - \langle x\rangle_2)^2}. \tag{B.1}$$

In the high-temperature limit $\beta \to 0$ a simple Taylor expansion yields

$$\langle x\rangle = \frac{1}{L}\left(\sum_i x_i - \beta\left(\sum x_i V_i - \sum x_i \sum \frac{V_i}{L}\right)\right) \tag{B.2}$$

where V_i is the random potential at position $x_i = i/L$. Therefore for (B.1) we obtain

$$\begin{aligned}\overline{(\langle x\rangle_1 - \langle x\rangle_2)^2} &= \Delta\beta^2 \frac{1}{L^2}\overline{\left(\sum_i x_i V_i - \sum_i x_i \sum \frac{V_i}{L}\right)^2} \\ &= (\Delta\beta)^2 \frac{\sigma^2}{120}\frac{(L^2-1)(L^2+10L+11))}{L^3}\end{aligned} \tag{B.3}$$

where in the last equality we have used the relation $\overline{V_i V_j} = \sigma^2 \min\{i, j\}$ which holds for Gaussian distributed forces with zero mean. For large L we recover expression (5),

$$\overline{(\langle x\rangle_1 - \langle x\rangle_2)^2} = \frac{\sigma^2}{120}(\Delta\beta)^2 L. \tag{B.4}$$

References

[1] Goldstein M 1969 *J. Chem. Phys.* **51** 3728
[2] Stillinger F H and Weber T A 1982 *Phys. Rev.* A **25** 978
[3] Kurchan J and Laloux L 1996 *J. Phys. A: Math. Gen.* **29** 1929
[4] Cavagna A 2001 *Europhys. Lett.* **53** 490
Grigera T S, Cavagna A, Giardina I and Parisi G 2002 *Phys. Rev. Lett.* **88** 055502 and references therein
[5] Mézard M, Parisi G and Virasoro M A 1987 *Spin Glass Theory and Beyond* (Singapore: World Scientific)
[6] Refregier Ph, Vincent E, Hammann J and Ocio M 1987 *J. Phys. France* **48** 1533
Vincent E, Bouchaud J-P, Hammann J and Lefloch F 1995 *Phil. Mag.* B **71** 489
[7] Bouchaud J-P and Dean D S 1995 *J. Physique* I *(France)* **5** 265
[8] Cugliandolo L and Kurchan J 1999 *Phys. Rev.* B **60** 922
[9] Derrida B 1981 *Phys. Rev.* B **24** 2613
[10] Hammann J, Vincent E, Dupuis V, Alba M, Ocio M and Bouchaud J-P 2000 *J. Phys. Japan* **69** 206 suppl A
[11] Jonson K, Vincent E, Hammann J, Bouchaud J-P and Norblad P 1998 *Phys. Rev. Lett.* **81** 3243
[12] Vincent E, Hammann J, Ocio M, Bouchaud J-P and Cugliandolo L F 1996 *Complex Behaviour of Glassy Systems (Lecture Notes in Physics)* ed M Rubí and C J Pérez (Berlin: Springer)
[13] Parker A and Normand V in preparation
[14] Fisher D S and Huse D A 1988 *Phys. Rev.* B **38** 386
Fisher D S and Huse D A 1988 *Phys. Rev.* B **38** 373
[15] Bray A J and Moore M A 1987 *Phys. Rev. Lett.* **58** 57
[16] Bouchaud J-P 2000 *Soft and Fragile Matter* ed M E Cates and M R Evans (Bristol: Institute of Physics Publishing)
[17] Bouchaud J-P, Dupuis V, Hammann J and Vincent E 2002 *Phys. Rev.* B **65** 024439 (*Preprint* cond-mat/0106539)
[18] Yoshino H, Lemaitre A and Bouchaud J-P 2001 *Eur. Phys. J.* B **20** 367–95
[19] Berthier L and Bouchaud J-P 2002 *Preprint* cond-mat/0202069
[20] Berthier L and Holdsworth P C W 2002 *Europhys. Lett.* **58** 35
[21] Sales M and Bouchaud J-P 2001 *Europhys. Lett.* **56** 181
[22] Sasaki M and Nemoto K 2000 *t J. Proc. Soc. Japan* **69** 2283
[23] Kawasaki M 2001 *J. Phys. Soc. Japan* **70** 1762–7
[24] Fisher D S and Huse D A 1991 *Phys. Rev.* B **43** 10728

[25] Sales M and Yoshino H 2002 *Phys. Rev.* E **65** 066131 (*Preprint* cond-mat/0203371)
[26] da Silveira R and Bouchaud J-P in preparation
[27] Kondor I 1989 *J. Phys. A: Math. Gen.* **22** L163
[28] Rizzo T 2001 *J. Phys. A: Math. Gen.* **34** 5531–49
[29] Rizzo T and Crisanti A 2002 Temperature chaos in the Sherrington–Kirkpatrick model *Preprint* cond-mat/0209333
[30] Ritort F 1994 *Phys. Rev.* B **50** 6844
[31] Ney-Nifle M and Young A P 1997 *J. Phys. A: Math. Gen.* **30** 5311
[32] Ney-Nifle M 1998 *Phys. Rev.* B **57** 492
[33] Billoire A and Marinari E 2000 *J. Phys. A: Math. Gen.* **33** L265 (*Preprint* cond-mat/0202473)
[34] Sasaki M and Martin O 2002 *Preprint* cond-mat/0206316
[35] Aspelmeier T, Bray A and Moore M 2002 Why temperature chaos in spin-glasses is hard to observe *Preprint* cond-mat/0207300
[36] Jönsson P E, Yoshino H and Nordblad P 2002 *Preprint* cond-mat/0203444 (accepted for publication in *Phys. Rev. Lett.* 2002)
[37] Picco M, Ricci-Tersenghi F and Ritort F 2001 *Phys. Rev.* B **63** 174412
Picco M, Ricci-Tersenghi F and Ritort F 2001 *Eur. Phys. J.* B **21** 211
[38] Bouchaud J-P, Comtet A, Georges A and le Doussal P 1990 *Ann. Phys., NY* **201** 285
[39] Bouchaud J-P and Georges A 1990 *Phys. Rep.* **195** 127
[40] Laloux L and Le Doussal P 1998 *Phys. Rev.* E **57** 6296
[41] Le Doussal P, Monthus C and Fisher D 1999 *Phys. Rev.* E **59** 4795
[42] Monthus C and Le Doussal P 2002 *Preprint* cond-mat/0202295
[43] Mézard M and Parisi G 1991 *J. Physique* I **1** 809
[44] Cugliandolo L F and Le Doussal P 1996 *Phys. Rev.* E **53** 1525
[45] Corberi F, Castellano C, Lippiello E and Zannetti M 2002 *Phys. Rev.* E **65** 046114, and references therein
[46] Luding S, Nicolas M and Pouliquen O 2000 A minimal model for slow dynamics: compaction of granular media under vibration or shear *Compaction of Soils, Granulates and Powders* ed D Kolymbas and W Fellin (Rotterdam: Balkema) p 241
[47] Lubensky D and Nelson D R 2001 *Phys. Rev.* E **65** 031917
[48] Mézard M 1990 *J. Phys. France* **51** 1831
[49] Parisi G 1990 *J. Phys. France* **51** 1595
[50] Bouchaud J-P and Orland H 1990 *J. Stat. Phys.* **61** 877
[51] Oshanin G, Mogutov A and Moreau M 1993 *J. Stat. Phys.* **73** 379
[52] Broderix K and Kree R 1995 *Europhys. Lett.* **32** 343
[53] Comtet A, Monthus C and Yor M 1998 *J. Appl. Prob.* **35** 255–71
[54] Komori T, Yoshino H and Takayama H 1999 *J. Phys. Soc. Japan* **68** 3387
Komori T, Yoshino H and Takayama H 2000 *J. Phys. Soc. Japan* **69** 1192
Komori T, Yoshino H and Takayama H 2000 *J. Phys. Soc. Japan* **69** 228
[55] Dupuis V, Vincent E, Bouchaud J-P, Hammann J, Ito A and Katori H A 2001 *Phys. Rev.* B **64** 174204
[56] Jönsson P E, Yoshino H, Nordblad P, Aruga Katori H and Ito A 2002 *Phys. Rev. Lett.* **88** 257204 (*Preprint* cond-mat/0112389)
[57] Feller W 1968 *An Introduction to Probability Theory and Its Applications* (New York: Wiley)
[58] Sasaki M, Dupuis V, Bouchaud J-P and Vincent E 2002 *Eur. J. Phys.* B **29** 469
[59] Carpentier D and Le Doussal P 2001 *Phys. Rev.* E **63** 026110
[60] Bouchaud J-P in preparation